Organic & Biomolecular Chemistry

RSC Publishing

PAPER

View Article Online
View Journal | View Issue

Cite this: *Org. Biomol. Chem.*, 2013, **11**, 1896

Helical peptides from VEGF and Vammin hotspots for modulating the VEGF–VEGFR interaction†

María Isabel García-Aranda,[a] Susana González-López,[a] Clara María Santiveri,[b] Nathalie Gagey-Eilstein,[c] Marie Reille-Seroussi,[c] Mercedes Martín-Martínez,[a] Nicolas Inguimbert,[c,d] Michel Vidal,[c,e] María Teresa García-López,[a] María Angeles Jiménez,[b] Rosario González-Muñiz[a] and María Jesús Pérez de Vega*[a]

Received 28th November 2012,
Accepted 18th January 2013

DOI: 10.1039/c3ob27312a

www.rsc.org/obc

The design, synthesis, conformational studies and binding affinity for VEGF receptors of a collection of linear and cyclic peptide analogues of the N-terminal α-helix fragments 13–25 of VEGF and 1–13 of Vammin are described. Linear 13(14)-mer peptides were designed with the help of an AGADIR algorithm and prepared following peptide solid-phase synthetic protocols. Cyclic peptide derivatives were prepared on-resin from linear precursors with conveniently located Glu and Lys residues, by the formation of amide linkages. Conformational analysis, CD and NMR, showed that most synthesized peptides have a clear tendency to be structured as α-helices in solution. Some of the peptides were able to bind a VEGFR-1 receptor with moderate affinity. In addition to the described key residues (Phe17, Tyr21 and Tyr25), Val14 and Val20 seem to be relevant for affinity.

Introduction

Angiogenesis is crucial for normal generation of new blood vessels, but it is also implicated in a number of pathological conditions,[1,2] such as cancer, rheumatoid arthritis, and diabetic retinopathy.[3,4] One of the key factors promoting angiogenesis is the Vascular Endothelial Growth Factor (VEGF) able to induce multiple biological actions of endothelial cells, like proliferation and migration, as well as vascular permeability enhancement.[5]

VEGF, and particularly its predominant isoform $VEGF_{165}$ (VEGF-A), exerts its pro-angiogenic action through its binding to specific receptors VEGFR-1 (Flt-1) and VEGFR-2 (KDR).[6–9] Recent studies have shown that both receptors are necessary for human tumor growth and metastasis formation.[7] Whilst VEGFR-2 appears to be directly involved in pathological angiogenesis, VEGFR-1 seems to work as a negative regulator of its activity,[7,10] although its implication in angiogenesis is clear.[11] VEGFR-1 and 2 receptors contain seven extracellular Ig-like domains connected by a single transmembrane helix to the intracellular tyrosine kinase domain. Most of the therapeutic strategies hitherto described are directed to the inhibition of the tyrosine kinase activity of the VEGF receptors.[12,13] There are indeed several compounds with this profile that are in advanced clinical trials for tumour angiogenesis treatment. Four small molecule tyrosine kinase inhibitors have now been approved by the FDA as anti-cancer agents – sunitinib, sorafenib, pazopanib and axitinib. An alternative approach is to disrupt VEGF–VEGFR interaction through neutralization of VEGF by monoclonal antibodies.[14–16] Bevacizumab is a humanized recombinant monoclonal antibody approved in 2004 as first line therapy for metastatic colorectal cancer, and was the first antiangiogenic agent launched to the market for the treatment of tumor angiogenesis. Additionally, different compounds have been described as inhibitors of the VEGF–VEGFR interaction through the binding to either VEGF[17] or VEGFRs[18,19] or co-receptors.[20,21] Most of these compounds have emerged from high throughput screening of peptide and diverse small-molecule libraries. VEGF and its receptors represent one of the best validated signaling pathways in angiogenesis,[22] however very little attention has been paid to the rational design of compounds to modulate the protein–protein interactions involved in the molecular recognition between VEGF and VEGFRs.[23–29] In this respect, disruption of the above-mentioned protein–protein interaction could be a valid target for the search for inhibitors of angiogenesis. Mutagenesis data indicated that the VEGF binding sites for VEGFR-1 and VEGFR-2 receptors are very similar.[30,31] Two

[a]*Instituto de Química Médica, CSIC, C/Juan de la Cierva 3, 28006 Madrid, Spain. E-mail: pdevega@iqm.csic.es*
[b]*Instituto de Química-Física Rocasolano, CSIC, C/Serrano 119, 28006 Madrid, Spain*
[c]*Université Paris Descartes, UFR des Sciences Pharmaceutiques et Biologiques, UMR CNRS 8638, 4 Avenue de l'Observatoire, Paris F-75270, France*
[d]*Université de Perpignan Via Domitia, Laboratoire de Chimie des Biomolécules et de l'Environnement, EA 4215, 52 Avenue P. Alduy, Perpignan F-66860, France*
[e]*UF Pharmacinétique et Pharmacochimie, GH Cochin – Hôtel Dieu – Broca, Hôpital Cochin, AP-HP, Paris, France*

†Electronic supplementary information (ESI) available: Synthetic procedures, compounds characterization, CD and NMR data. See DOI: 10.1039/c3ob27312a

main hot-spots have been identified at the interaction interface between VEGF and these receptors. These are fragments of $VEGF_{17–25}$, located at the N-terminal and $VEGF_{81–91}$, located at loop 3.[32–36] We have recently reported the preparation of cyclic peptide analogues of the second of these two hot-spots, $VEGF_{81–91}$.[37,38] Molecular modeling and ^1H NMR studies on these peptides indicated a tendency to be structured around the central β-turn of the $VEGF_{81–91}$ β-hairpin and some of them showed significant affinity for VEGFR-1, thus supporting the design of mimics of this fragment as a valid approach to disrupt the VEGF–VEGFR-1 interaction.

Concerning the less explored N-terminal fragment of $VEGF_{17–25}$, D'Andrea and co-workers have reported a 15-mer analogue of $VEGF_{14–28}$ (Ac-KLTWMELYQLAYKGI-NH_2) that exhibits stable helical structure in solution, and pro-angiogenic properties both *in vitro* and *in vivo*.[39,40] More recently, the same authors described the preparation of a new peptide analogue (Ac-KLTWQELYQLKYKGI-NH_2) that shows anti-angiogenic properties.[41] Both peptides bind to the membrane of endothelial cells, as observed in cellular assays, but no binding assays with isolated receptors were reported. Within the VEGF-A fragment 17–25, a Phe17 residue has been identified as key for the interaction with VEGF receptors 1 and 2, while Tyr21 and Tyr25 seem to be important for the stabilization of the α-helical structure.[34] Moreover, this fragment has been also located at the interaction interface of VEGF and the Fab fragment of the monoclonal antibody bevacizumab,[42] and some other antibodies and peptides.[15,36]

Vammin is a VEGF protein isolated from snake venom that exhibits potent antiangiogenic activity both *in vitro* and *in vivo*, and proved to be specific for the VEGFR-2 receptor in a surface plasmon resonance (SPR) binding assay.[43] In addition to VEGF, Vammin could be also considered a source of peptide analogues for VEGF–VEGFR modulators. The crystal structure of Vammin, reported by Morita and co-workers, revealed high structural similarities with VEGF-A,[44] and these authors centered their structural studies particularly on the Vammin fragment 69–80, which corresponds to $VEGF_{81–91}$.

Based on all the above precedents, we describe herein our efforts towards the *de novo* design of helical peptides able to mimic $VEGF_{13–25}$ and $Vammin_{1–13}$ fragments, selected as the minimum sequence to maintain the native helix conformation. Our main goal is to interfere with the VEGF–VEGFR interaction and try to identify key elements driving the molecular recognition between these two proteins. The small set of designed peptides adopted the desired α-helical structures, similar to those of the parent fragments in the native proteins, as confirmed by CD and ^1H NMR studies. Moreover, most of them are able to interact with the VEGFR-1 receptor.

Results

Design

Fragments of VEGF-A (13–25) and Vammin (1–13), with helical structure within the respective native protein, were taken as models for the search for new modulators of the VEGF–VEGFR interaction. For the design of $VEGF_{13–25}$ analogues, key amino acids Phe17, Tyr21 and Tyr25 (corresponding to residues 5, 9 and 13 in the designed peptides) were maintained while the other residues were replaced. Alignment of the N-terminal regions of VEGF-A and Vammin permitted the identification of the fragment 1–13 of Vammin as the sequence corresponding to the $VEGF_{13–25}$ fragment. In this case, residues Phe5, His9, and Ala13, located at the equivalent positions identified as key in $VEGF_{13–25}$, were kept intact and only the rest of the residues were modified. From the indicated fragments, virtual collections of linear peptides were generated by replacing each of the modifiable residues by the 20 proteinogenic amino acids. Then, we examined the helical character of each virtual peptide using an AGADIR10 algorithm.[45]

Residues that increased the helical character of the peptide were then combined to create a second-generation virtual library. From this virtual collection, two peptides were chosen to be prepared: one analogue of $VEGF_{13–25}$, compound **2**, and one of $Vammin_{1–13}$, **6** (Fig. 1). According to AGADIR prediction, these analogues have higher tendency to adopt helical conformations (≥60%), than the native sequences **1** and **5** (Fig. 1). An important issue regarding purification as well as conformational and biological studies of peptides is their aqueous solubility. Taking into account that modifications to increase helicity are often associated with a decrease in solubility, four new peptide analogues (**3**, **4**, **7** and **8**), which contain more polar residues (Ser), were selected. These peptides presumably would be slightly more soluble in aqueous media than the previous analogues, as estimated by their log *S* values (calculated by the AlOGPS 2.1 program),[46,47] while still maintaining a good predisposition to adopt helical conformations.

In addition, compounds **10** and **12**, two constrained cyclic peptide analogues of $VEGF_{13–25}$, were designed (Fig. 2). In this case, the strategy to fix the α-helix involved crosslinking amino acid side-chains at relative positions *i* and *i* + 4, corresponding either to residues 3 and 7 (A) or 7 and 11 (B) of the peptide, situated at the opposite face to that containing the residues reported as important for the molecular recognition. The cyclization was performed through the generation of

Comp. Nº	Sequence														AGADIR Predicted helix Percentage (%)
	1	2	3	4	5	6	7	8	9	10	11	12	13	14	
	13	14	15	16	17	18	19	20	21	22	23	24	25	26	
1: $VEGF_{13-25}$	Ac-E	V	V	K	F	M	D	V	Y	Q	R	S	Y-NH_2		2.5
2	Ac-E	V	Q	K	F	L	E	V	Y	L	R	L	Y-NH_2		65
3	Ac-S	S	Q	K	F	L	E	V	Y	Q	R	L	Y	N-NH_2	27
4	Ac-S	S	Q	K	F	L	E	V	Y	L	R	L	Y	N-NH_2	32
	1	2	3	4	5	6	7	8	9	10	11	12	13		
5: $Vammin_{1-13}$	Ac-E	V	R	P	F	L	E	V	H	E	R	S	A-NH_2		0.3
6	Ac-D	V	R	R	F	L	E	V	H	L	R	L	A-NH_2		60
7	Ac-D	L	R	A	F	L	E	Q	H	L	R	S	A-NH_2		32
8	Ac-S	V	R	R	F	L	E	A	H	L	R	L	A-NH_2		41

Fig. 1 Sequences of $VEGF_{13–25}$, $Vammin_{1–13}$ and designed analogues **1–8**.

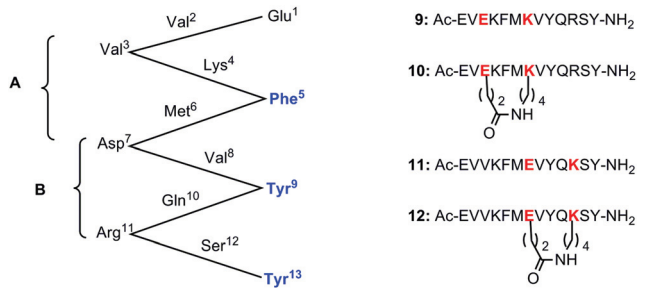

Fig. 2 Cyclic constrained $VEGF_{13–25}$ peptide analogues **10** and **12**, and the corresponding linear precursors **9**, **11**.

covalent amide bridges from conveniently situated Glu and Lys residues, leading to lactam constrained cyclic peptides. This approach has been widely reported as a successful strategy for the stabilization of helical conformations.[48–50] For comparative purposes, it is also planned to study linear precursors **9** and **11**.

Synthesis

The synthesis of the designed peptides (Fig. 1 and 2) was performed in parallel, following solid-phase protocols, using a Rink amide MBHA polystyrene resin and an Fmoc/^{t}Bu strategy. To prevent aggregation problems, and to favor intramolecular cyclization when required, a low load resin (0.34 mmol g^{-1}) was used. All compounds were isolated as C-terminal amides and acetylated at the N-terminal.

Cyclic compounds **16** and **18** were prepared by formation of a side-chain-to-side-chain glutamate–lysine amide linkage, from linear precursors **15** and **17** respectively (Scheme 1). The glutamic acid residue was always placed towards the N-terminal side of the peptide, because a Glu-X-X-X-Lys arrangement promotes higher helicity than the opposite Lys-X-X-X-Glu organization, as reported by Mills *et al.* for a series of polyarginine α-helical peptidomimetics.[49] Glu and Lys side-chains were conveniently protected with allyl and Alloc groups, respectively, suitable for orthogonal deprotection before on-resin cyclization. After N-terminal acetylation, and Pd-catalyzed deallylation of the linear precursors **13** and **14**, lactamization was performed with the assistance of microwave irradiation, using PyAOP as a coupling agent.[51–53] 15% TFE was used as a cosolvent of DCE, to stabilize the helix conformation and to facilitate the cyclization. The reaction was accomplished in 1 h for both derivatives, leading to the corresponding cyclic compounds. After cleavage from the resin final cyclic peptides were isolated, lyophilized and purified by semipreparative HPLC in good yields. Linear peptide analogues were obtained after a sequence comprising Fmoc-deprotection, acetylation, removal of allyl groups and final cleavage from the resin. The expected peptides **9–12** were not isolated as such, but as sulphones, compounds **15–18** (Scheme 1) due to overoxidation of the Met side-chain.[54] NMR and mass spectra data of the isolated compounds agreed with the sulphone structure (ESI†).[55]

Conformational analysis by circular dichroism

The tendency of the designed peptides to adopt helical conformations was first examined by circular dichroism (CD). CD spectra of compounds **1–8**, **15–18** in aqueous solution are indicative of mainly disordered peptides. The helix populations estimated from the observed ellipticity ([θ]) at 222 nm in water at 5 °C are less than 10% for all peptides, except for peptides **4**, **7**, **16** and **18** with helix populations in the 10–25% range. These results contrast with the helical percentages of up to 30–65% predicted from the sequence by AGADIR. These discrepancies arise, in part, from the low solubility shown by most of the peptides, particularly, the most hydrophobic (**3** and **8**), and from inaccurate estimations of peptide concentrations from UV absorption values, especially in the case of the aromatic-lacking Vammin analogues, which translate into inaccurate ellipticity values ([θ], see Methods). All peptides become more helical in the presence of TFE, as shown by their CD spectra that display the helix-characteristic double minimum at 208 and 222 nm (Fig. 3 and S1–3†). This indicated that the designed peptides have high tendency to be helical in the appropriate environment.

NMR conformational studies

To get further details of the structures adopted by the VEGF and Vammin analogues, we performed an NMR structural study of the peptides. Taking into account that CD indicated very low helical percentages for all the peptides in aqueous solution, together with their low solubility, we decided to study the peptides in the presence of trifluoroethanol.

The VEGF and Vammin analogues were demonstrated to adopt helical structures in the mixed TFE–H_2O solvent by the set of NOEs, which included the non-sequential helix-characteristic $d_{\alpha N(i,\ i+3)}$, $d_{\alpha N\ (i,\ i+4)}$ and $d_{\alpha\beta\ (i,\ i+3)}$ NOEs (see NOE summaries in Fig. S7–S9†). Some of these non-sequential NOE cross-peaks are seen in the NOESY spectral region shown in Fig. 4 for compound **2**.

Further evidence to support the helical structure of the peptides came from the $^1H_\alpha$ and $^{13}C_\alpha$ chemical shifts, which depend on the ϕ and ψ dihedral angles.[56] Thus, the profiles of conformational shifts ($\Delta\delta = \delta^{observed} - \delta^{random\ coil}$, ppm; where $\delta^{random\ coil}$ were taken from Wishart *et al.*[57]) presented for all the peptides are characteristic of helical structures, *i.e.*, negative values for the H_α protons (Fig. 5) and positive values for C_α (Fig. S4–6†). The absolute values for the central residues are larger than those at the N- and C-termini, which indicates that, as commonly found in linear helical peptides (*i.e.* **6**), the helices are frayed at both ends. This fraying effect is more apparent at the N-terminus of compound **5**, the native fragment of Vammin, which is explained by the presence of a Pro residue at position 4 (Fig. 1). This Pro probably distorts the ϕ and ψ dihedral angles characteristic of α-helices and, prevents the formation of the first H-bond of the helix, between this residue and Glu1.

Apart from the fraying effect, the magnitudes of the conformational shifts differ among the different peptides (Fig. 5).

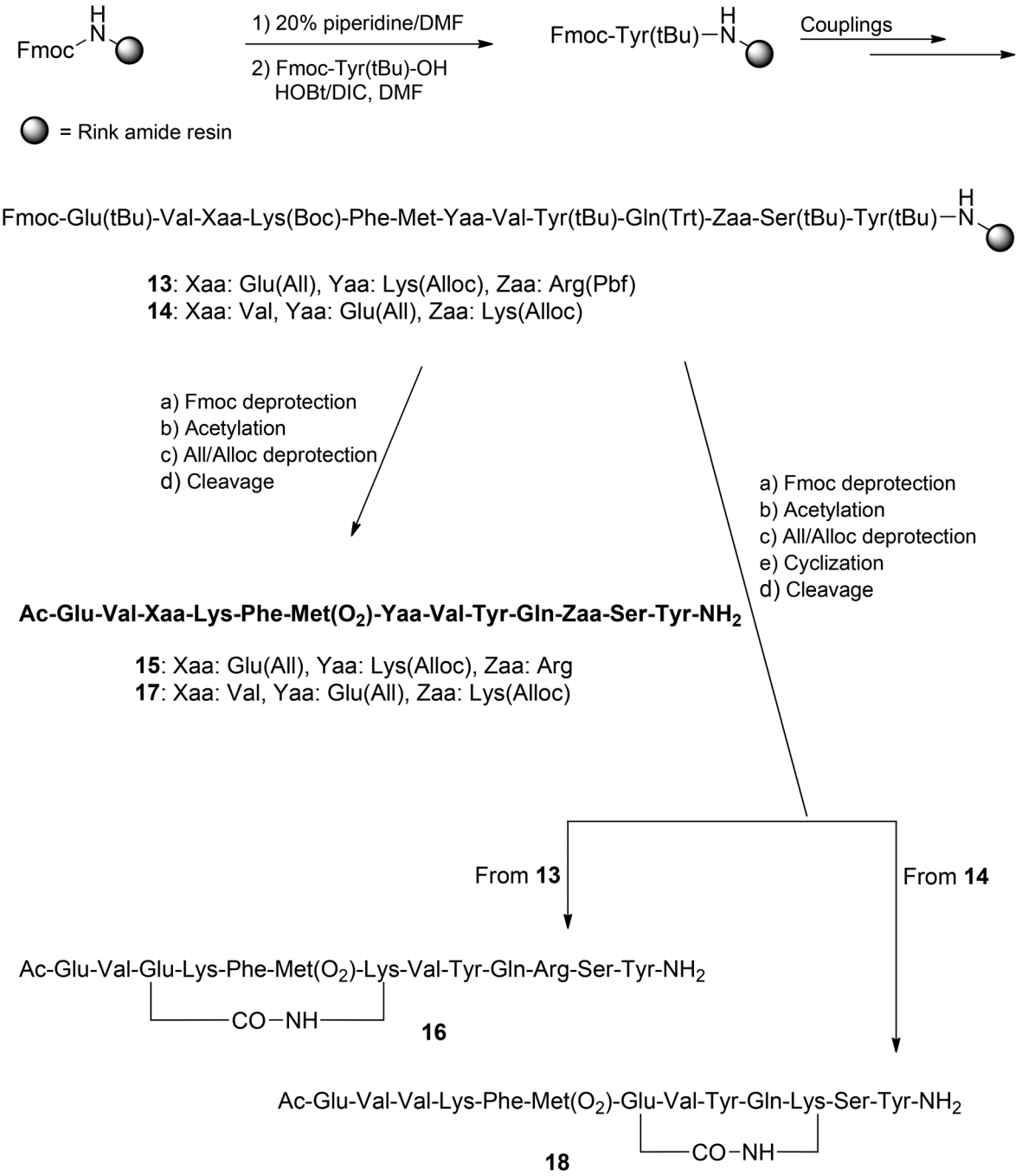

Scheme 1 Synthesis of amide-bridged cyclic peptides **16** and **18**. (a) 20% piperidine–DMF; (b) Ac_2O, DIEA–DMF; (c) $PhSiH_3$, $Pd(PPh_3)_4$, DCM; (d) TFA–EDT–H_2O–TIS (94 : 2.5 : 2.5 : 1); (e) PyAOP–HOAt, DIEA, DMF, 120°, MW.

The larger the magnitudes, the more populated are the helices. Based on the averaged $\Delta\delta_{H\alpha}$- and $\Delta\delta_{C\alpha}$-values (Fig. 5), the peptides can be qualitatively ranked according to their helical populations. Additionally, the percentages of helix adopted for each peptide can be quantitatively estimated from the averaged $\Delta\delta_{H\alpha}$-values, as previously described[58,59] (Table 1). Qualitatively, the ranking of the peptides in terms of theoretical (Fig. 1) and experimental helicity is coincident. In general, the peptides with larger helix populations show a larger number of non-sequential NOEs.

To visualize the helices adopted by the studied peptides, we performed structure calculations (see Experimental methods). The resulting structures are well defined (the range of average RMSD for backbone atoms is 0.1–0.4 Å; see Table ST13 in ESI†) and, as deduced from analysis of chemical shifts (see above), show some fraying at the ends (Fig. S10–11†). The C-termini are generally better defined in the VEGF-A than in the Vammin analogues. This is probably due to the interactions between the aromatic residues F5/Y9/Y13, all at the same helix face, being more stabilizing than the corresponding

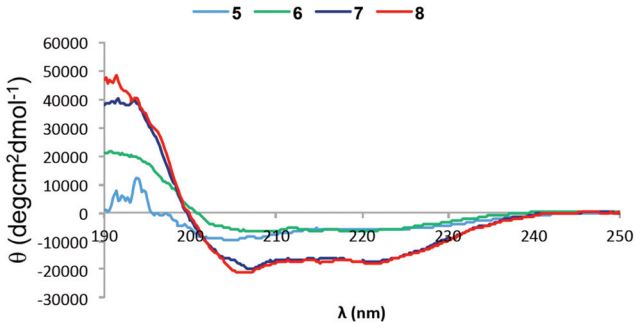

Fig. 3 CD spectra for Vammin$_{1-13}$ analogues **5–8**, in 30% TFE–H_2O at pH 5.5 and 5 °C.

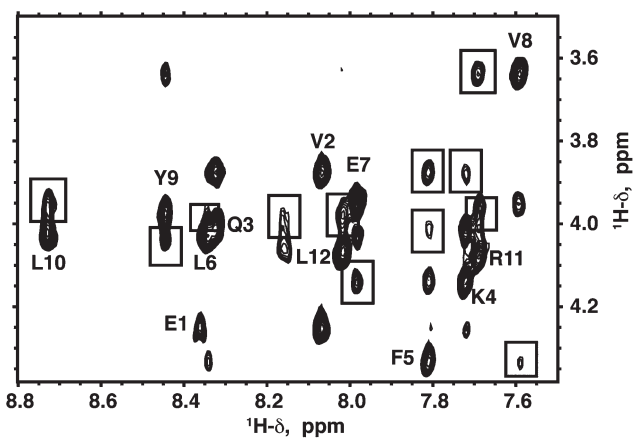

Fig. 4 Selected NOESY spectral region for peptide **2** in 30% TFE–H_2O at pH 5.5 and 5 °C. The intra-residual H_α-NH cross-peaks are labeled and the non-sequential $d_{\alpha N(i,\ i+3)}$ and $d_{\alpha N(i,\ i+4)}$ boxed. The sequential $d_{\alpha N(i,\ i+1)}$ are not labeled.

interactions (F5/H9/A13) in the Vammin analogues, as seen in Fig. 6 for VEGF analogue **2** and Vammin analogue **8**. Concerning the N-termini, the helices of the VEGF-A analogues with a better N-cap residue, such as the N-terminal Glu in peptides **1** and **2**, are less frayed than other compounds, for example, compounds **3** and **4** with two consecutive Ser residues at the N-end (Table 1). Among the Vammin analogues, the most disordered at the N-terminus is peptide **5** with a Pro at position 4, as deduced from conformational shifts (see above).

Concerning the bridged VEGF peptides **16** and **18** (Fig. 2), the helices adopted by the two peptides with an $i/i + 4$ bridge are more populated than their corresponding linear analogues **15** and **17**, respectively, but, peptide **16** shows a lower helix population than peptide **18.**

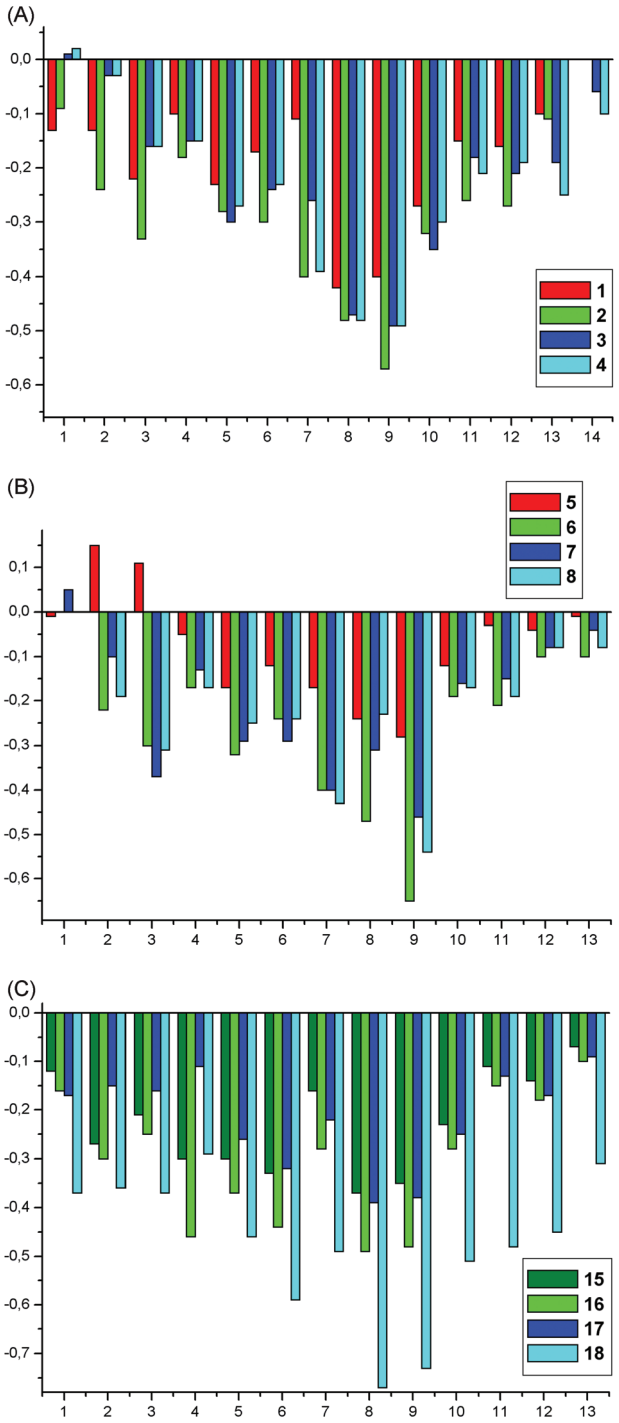

Fig. 5 Histogram showing the $\Delta\delta_{H\alpha}$ values ($\Delta\delta_{H\alpha} = \delta_{H\alpha}^{observed} - \delta_{H\alpha}^{RC}$, ppm) as a function of the sequence number for: (A) VEGF$_{13-25}$ analogues **1–4**, (B) Vammin$_{1-13}$ analogues **5–8**, and (C) VEGF$_{13-25}$ analogues **15–18**.

Table 1 Helix populations estimated for peptides **1–8**, **15–18** in 30% TFE at pH 5.5 and 25 °C from $\Delta\delta_{H\alpha}$-values as described in Methods

Peptide	1	2	3	4	5	6	7	8	15	16	17	18
Av. $\Delta\delta_{H\alpha}$ (ppm)	−0.20	−0.29	−0.26	−0.27	−0.14	−0.28	−0.23	−0.24	−0.23	−0.30	−0.22	−0.48
% Helix	51	74	67	69	36	72	59	62	59	77	56	100

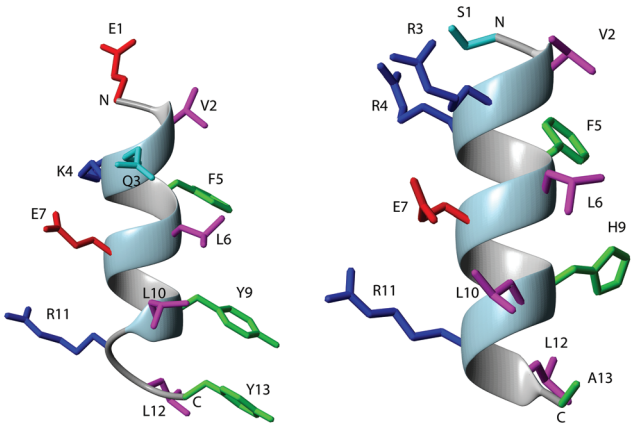

Fig. 6 NMR lowest target function structures of VEGF analogue **2** (left) and Vammin analogue **8** (right): backbone atoms are shown as ribbons. Side chains are colored in red for the negatively charged residues, in blue for the positively charged residues, in cyan for the polar residues, in magenta for the hydrophobic residues (Val/Leu), and in green for the residues reported as key for the interaction with VEGF receptors. Hydrogen atoms are not shown. All the residues are labeled and the N- and C-ends are indicated. Side chains of Val8 and Ala8 are not seen because they lie behind the ribbon.

Table 2 Inhibitory potency of peptides **1–8**, **15–18** on VEGFR-1. Displacement assays

Compound	Sequence	%Inhibition[a] ECD	IC_{50}[b](μM)
1	Ac-EVVKFMDVYQRSY-NH_2	20 ± 3	—
2	Ac-EVQKFLEVYLRLY-NH_2	9 ± 7	—
3	Ac-SSQKFLEVYQRLYN-NH_2	N/A[c]	—
4	Ac-SSQKFLEVYLRLYN-NH_2	N/A	
5	Ac-EVRPFLEVHERSA-NH_2	46 ± 9	47 ± 6
6	Ac-DVRRFLEVHLRLA-NH_2	62 ± 18	—
7	Ac-DLRAFLEQHLRSA-NH_2	N/A	—
8	Ac-SVRRFLEAHLRLA-NH_2	42 ± 6	—
15	Ac-EVEKFM(O_2)KVYQRSY-NH_2	62 ± 15	95 ± 17
16	Ac-EV-*c*(NH-CO)^{3,7}[EKFM(O_2) K] VYQRSY-NH_2	56 ± 11	36 ± 9
17	Ac-EVVKFM(O_2)EVYQKSY-NH_2	74 ± 8	43 ± 9
18	Ac-EVVKFM(O_2)-*c*(NH-CO)^{7,11} [EVYQK]SY-NH_2	53 ± 11	52 ± 6

[a] Activity corresponds to the percentage of biotinylated VEGF165 displaced by a concentration of peptide of 100 μM on the whole extracellular domain (ECD, D1–D7) of VEGFR-1. [b] Inhibitory concentration able to displace 50% binding of biotinylated VEGF165 on D1–D3 VEGFR-1. [c] N/A = no affinity observed.

Binding affinity for VEGFR-1

Synthesized peptides were evaluated for their ability to displace biotinylated $VEGF_{165}$, in a chemiluminescent assay relying on competition between tested compounds and biotinylated $VEGF_{165}$ for binding to the extracellular domain of recombinant VEGFR-1[28,60] (D1–D7, Table 2). Some of the best compounds were selected for dose–response binding studies on the D1–D3 domain of the VEGFR-1 receptor, the specific domains for VEGF binding.

Some of the prepared peptides exhibited good inhibition percentages. Thus, for VEGF analogues, the best results were shown by cyclic peptides **16** and **18** together with their linear parent compounds **15** and **17**, while AGADIR-based designed peptides, **2–4**, did not show significant binding. Concerning Vammin analogues, **5–8**, the parent Vammin 1–13 native sequence, **5**, together with analogues **6** and **8**, showed significant affinity for VEGFR-1, with values of the same order as those found for the VEGF derivatives (Table 2).

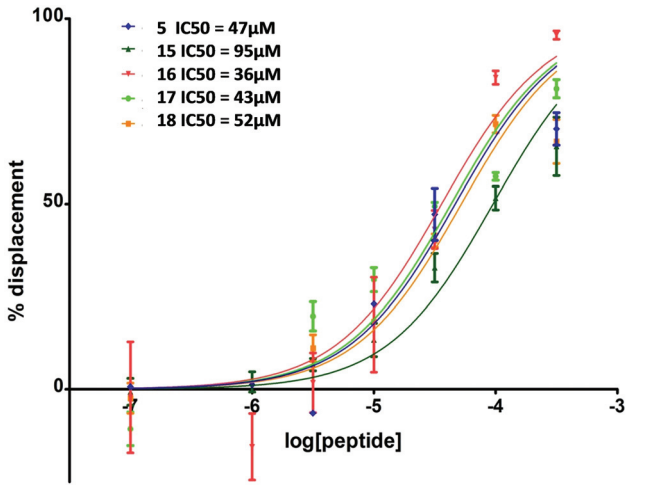

Fig. 7 Dose–response curves for peptides **5**, **15–18** on VEGF-1 D1–D3 displacement assays.

Dose–response experiments to determine IC_{50} values for most compounds that have shown significant affinity for the VEGFR-1 receptor were performed. Cyclic constrained VEGF analogues **16** and **18** and their parent linear precursors, **9** and **17**, showed good binding affinities. Cyclic analogue **16** having the conformational restriction closer to the N-terminus of the sequence exhibited the best IC_{50} value found for this collection of peptides (Table 2, Fig. 7).

Discussion and conclusions

A small collection of linear and cyclic peptide analogues (**1–8**, **15–18**) of the fragment 13–25 of VEGF, previously identified as a hot-spot of the VEGF–VEGFR interaction, and of the corresponding fragment of Vammin, 1–13, have been designed and synthesized by solid-phase techniques. NMR conformational studies (chemical shift deviation and non-sequential NOE) showed that, in TFE–H_2O solution, these peptides adopted the desired native-like helical conformation. In general, and as expected, the designed peptides were more structured than the parent compounds **1** and **5**.

When evaluated as inhibitors of the VEGF–VEGFR interaction most peptides proved to bind to the VEGFR-1 receptor, the VEGF cyclic analogue **16** exhibiting the best IC_{50} value. A combined analysis of structural and biological results indicated that to interact with VEGFR-1, the peptides needed to have a certain tendency to be helical, but once a minimum helical population is reached the affinity of the peptides does not increase with increments in helicity. Detailed comparison

among the sequences of the designed analogues and the native $VEGF_{17–25}$ and $Vammin_{1–13}$ native sequences indicates that the two N-terminal residues, Glu1 and Val2, of **1** and **5** could be directly participating in the VEGF–VEGFR interaction. Thus, VEGF analogues **3** and **4**, in which Val2 has been replaced by a Ser, and Vammin analogue **7**, in which it has been replaced by Leu, showed no affinity for the VEGFR-1 receptor. Although this last change is more conservative, the concomitant replacement of Val8 by Gln in **7** could also contribute to the lack of affinity. This Val residue is in the same face of the helix as key residues Phe17, Tyr21, suggesting the importance of a hydrophobic region for the interaction. On the other hand, the Glu1 residue may play a stabilizing role on the helical structure, as it is able to form H-bonds between its side chain and unpaired main-chain NH and CO groups of the first turn. Accordingly, it can be replaced by residues with N-cap properties as Ser or Asp (compare compound **5** with **6** and **8**).[61] In the case of peptides **3** and **4**, the extra C-terminal residue (Asn) might also be responsible for the drop in affinity. As for the inhibition value found for analogue **2** was not very reliable, taking into account the low water solubility and the high ability for aggregation shown by this peptide at the concentration used in the binding assay.

Cyclic constrained VEGF analogues **16** and **18** and their parent linear precursors **15** and **17** showed good VEGFR-1 affinity values. Linear peptides **15** and **17** showed 3–4 fold increased affinity for VEGFR-1 over the native fragment **1**, and a slightly higher helicity. Compound **15** encompasses two radical, non-conservative changes: Val3 has been replaced by Glu, and Asp7 by Lys, while in the case of peptide **17**, the changes are much more conservative: Asp7 by Glu and Arg11 by Lys. However, all these modifications improve the affinity for the receptor, suggesting that the original residues are not very important for binding. Therefore, the improved affinities of **15** and **17** could be ascribed to the increased helical character, since the formation of ionic bridges between Glu and Lys residues could contribute to the stabilization of their helical conformation (Table 2, Fig. 7).[62] Cyclic analogues **16** and **18** also proved to have more helical character than the parent compound **1**, and more than linear precursors **15** and **17**. As already mentioned, cyclic peptide **16** is the best compound within this collection in terms of affinity for the VEGFR-1. However, peptide **18**, with higher helicity than **16**, showed less affinity for the receptor. The masking of the basic character of the Arg11 residue, by forming the lactam cycle, could be responsible for the slight drop in affinity observed for **18** compared with its parent linear compound **17** that still has a basic Lys residue at the place of Arg11. The results found for compound **5**, native sequence of Vammin, together with analogues **6** and **8**, showing non-negligible IC_{50} values for binding with VEGFR-1, suggest that the specificity of Vammin for VEGFR-2 *versus* VEGFR-1[43] seems not to rely on this part of the Vammin molecule (Table 2, Fig. 7).

Compared with the previously prepared analogues of the $VEGF_{81–91}$ fragment,[37,38] it can be said that the affinities found for the helical peptides described here are slightly better. This can be attributed to the fact that their spatial conformation mimics better the helical conformation adopted by the parent native fragments in the protein, while in the $VEGF_{81–91}$ analogues only the β-turn of the native β-hairpin was mimicked. This is also in accordance with the improved ability to displace the VEGFR-1–VEGF interaction observed for the helical 16–27 fragment of VEGF as compared to the $VEGF_{61–68}$ sequence, proving once more that the 16–27 helical fragment constitutes a hot-spot in the VEGF–VEGFR-1 interaction.[24]

In summary, Vammin analogues **5**, **6** and **8**, and cyclic constrained VEGF-A derivatives **16** and **18** as well as their precursors **15** and **17** were able to interfere with the process of VEGF–VEGFR-1 recognition. Compound **16**, one of the peptides with higher helical character, showed the best IC_{50} value in the binding assay. As a conclusion, it can be inferred that $VEGF_{13–25}$, corresponding to one of the identified hot-spots for the VEGF–VEGFR interaction, and its homologue $Vammin_{1–13}$, can be taken as templates for the design of peptide mimics able to interfere with the interaction of VEGF with its receptors. The detailed analysis of the peptide sequences suggests a role for Glu1, as a helix initiator, and for Val2 and Val8 residues as relevant for the interaction with VEGFR-1, likely being important as a hydrophobic patch, together with Phe5, Tyr9, Tyr13. In addition, the obtained results suggest that the specificity of Vammin for the VEGFR-2 receptor does not rely on the N-terminal region of the molecule, although minor modifications in this fragment can lead to the loss of VEGFR-1 affinity (*i.e.*, compound **7**). These results encourage us to prepare more VEGF and Vammin analogues to selectively interfere with the VEGF–VEGFR-1 or VEGF–VEGFR-2 interaction, which can constitute interesting tools in pharmacology.

Experimental

Synthesis of linear and cyclic derivatives 1–8, 15–18. General procedure

Resin bound peptides were synthesized by conventional Fmoc solid-phase chemistry on an MBHA-Rink amide resin.

Resins were swollen in DCM/DMF/DCM/DMF (4 × 0.5 min). All compounds were synthesized manually in parallel on resin, following the Fmoc/*t*Bu strategy, using Fmoc-Glu(O*t*Bu)-OH, Fmoc-Val-OH, Fmoc-Lys(Boc)-OH, Fmoc-Phe-OH, Fmoc-Leu-OH, Fmoc-Ile-OH, Fmoc-Met-OH, Fmoc-Arg(Pbf)-OH, Fmoc-His(Trt)-OH, Fmoc-Asp(O*t*Bu)-OH, Fmoc-Tyr(*t*Bu)-OH, Fmoc-Pro-OH, Fmoc-Gln(Trt)-OH, Fmoc-Ser(*t*Bu)-OH, Fmoc-Asn(Trt)-OH, Fmoc-Ala-OH, Fmoc-Lys(Alloc)-OH or Fmoc-Glu(All)-OH as required.

In each coupling step, the appropriate Fmoc amino acid (1.5 equiv.) was treated with HOBt/DIC (1.5 equiv.) in anhydrous DMF or with HCTU/DIEA (2 equiv.). Couplings were allowed to proceed at room temperature overnight or for 1 h, respectively. The coupling efficiency was monitored by ninhydrin or chloranil test, and when necessary repeated with a fresh portion of Fmoc-amino acid and the indicated coupling reagents. After each coupling step, the Fmoc group was

removed by treatment with 20% piperidine in DMF (3 × 10 min). The resin was washed and drained with DMF/DCM/DMF/DCM (4 × 0.5 min).

For amide bridge formation, after removing Alloc and OAll protecting groups, the linear-resin-bound derivative (100 mg, 0.034 mmol) was treated with a solution of PyAOP (177 mg, 0.34 mmol), HOAt (46 mg, 0.34 mmol), DIEA (0.12 ml, 0.68 mmol) in anhydrous DMF (2 ml). The reaction was allowed to proceed under microwave irradiation for 1 h until ninhydrin test was negative. The resin was washed and drained with DMF/DCM/DMF/DCM (4 × 0.5 min).

Before cleavage from the resin, all derivatives were acetylated by treatment with a mixture of Ac_2O–DIEA in DMF (4 × 10 min) and then washed with DMF and DCM. For cyclic analogues, acetylation was performed before Alloc and OAll deprotection prior to cyclization. Finally, the resin was treated with the cleavage cocktail TFA–EDT–H_2O–TIS (94 : 2.5 : 2.5 : 1) for 5 h at room temperature. The filtrates were precipitated from diethyl ether, centrifuged and lyophilised, and the resulting mixture was purified by reverse phase semipreparative HPLC to obtain the peptides **1–8**, **15–18** in high purities (>98%, HPLC-MS data) and 1–9% overall yield (calculated on the bases of resin substitution). See ESI† for details.

Circular dichroism spectroscopy

CD spectra were recorded on a Jasco J-810 instrument equipped with a Peltier temperature control unit, at 5 °C both in H_2O and in 30% TFE–H_2O solutions.

2D NMR spectroscopy

Samples were prepared by dissolving the lyophilized peptide (~1 mg) in 0.4 ml of H_2O–D_2O 9 : 1 v/v, adjusting the pH to 5.5 by adding minimal amounts of NaOD or DCl, and adding the amount of deuterated TFE (0.17 ml) necessary to give a TFE/water ratio of 30 : 70 in volume. Resulting peptide concentrations were about 1 mM. pH was measured with a glass microelectrode and not corrected for isotope effects. The temperature of the NMR probe was calibrated using a methanol sample. Sodium 2,2-dimethyl-2-silapentane-5-sulfonate (DSS) was used as an internal reference. NMR spectra were acquired at 25 °C in a Bruker AV-600 spectrometer operating at a proton frequency of 600.13 MHz and equipped with a cryoprobe. As previously reported,[63] phase-sensitive two-dimensional correlated spectroscopy (COSY), total correlated spectroscopy (TOCSY), nuclear Overhauser enhancement spectroscopy (NOESY) spectra and ^1H–^{13}C heteronuclear single quantum coherence spectra (HSQC) at natural ^{13}C abundance were recorded by standard techniques using presaturation of the water signal and the time-proportional phase incrementation mode. NOESY mixing times were 150 ms and TOCSY spectra were acquired using 60 ms DIPSI2 with a z filter spin-lock sequence. Acquisition data matrices were defined by 2018 × 512 points in t_2 and t_1, respectively. Data were processed using the standard TOPSPIN program.[64] The 2D data matrix was multiplied by either a square-sine-bell or a sine-bell window function with the corresponding shift optimized for every spectrum and zero-filled to a 2K × 1K complex matrix prior to Fourier transformation. Baseline correction was applied in both dimensions. The 0 ppm ^{13}C δ-value was obtained indirectly by multiplying the spectrometer frequency that corresponds to 0 ppm in the ^1H spectrum, assigned to an internal DSS reference, by 0.25144953.[65] Standard sequential assignment methods[66,67] were applied to assign the ^1H NMR signals of the peptides. Then, the ^{13}C resonances were straightforwardly assigned based on the cross-correlations observed in the HSQC spectra between the proton and the bound carbon (^1H and ^{13}C chemical shifts for all the compounds are listed in Tables ST1–ST12 as ESI†).

NMR structure calculation

Distance constraints were derived from the 2D 150 ms mixing time NOESY spectra. The NOE cross-peaks were integrated by using the automatic integration subroutine of the SPARKY program[68] and then calibrated and converted to upper-limit distance constraints within the CYANA program. After calibration, we excluded from the input list of distance constraints those for which contribution of random conformations can be large, *i.e.* intra-residual and sequential, except for the $d_{\mathrm{NH}i-\mathrm{NH}i+1}$, which are characteristic of helices and absent or very weak in random conformations. ϕ and ψ angle restraints were obtained from $^1H_\alpha$, $^{13}C_\alpha$ and $^{13}C_\beta$ chemical shifts using the TALOS program.[69] The ϕ angles for those residues for which the derived angle restraints were ambiguous were restricted to the −180° to 0° range. A total of 50 structures were calculated using the standard annealing strategy of the CYANA program.[70] The 20 structures with the lowest target function values were selected and energy-minimised within the CYANA program. The structures were examined using the program MOLMOL.[71]

Chemiluminescent competition assays

The surface of a white high-binding 96-well microplate was coated with 100 µl of phosphate-buffered saline solution (PBS, pH 7.4) containing either VEGFR-1 D1–D3/Fc Chimera (20 ng per well) or VEGFR-1 D1–D3/Fc chimera (15 ng per well) and incubated at 4 °C overnight. After three washes with 250 µl of PBS 0.1%, (v/v) Tween 20 (buffer A), the plate was blocked by 200 µl of PBS with 3% (w/v) of BSA and stirred at 37 °C for 2 h. The plate was washed three times with buffer A. Then, 100 µl of a solution of bt$VEGF_{165}$ at 131 pM (5 ng mL^{-1}) and the tested compounds at various concentrations diluted in PBS containing 1% DMSO were added to each well. After 3 h stirring at 37 °C, the plate was washed four times with buffer A and 100 µl of streptavidin–horseradish peroxidase diluted at 1 : 8000 in PBS containing 0.1% (v/v) Tween 20 and 0.3% (w/v) BSA were added per well. After 1 h of incubation at 37 °C in the dark and stirring, the plate was washed five times with 250 µl of buffer A and 100 µl of the chemiluminescent substrate were added. The remaining bt-$VEGF_{165}$ was detected by chemiluminescence, which was quantified. The percentages of bt$VEGF_{165}$ displacement were calculated by the following formula: percentage of displacement = 100 × [1 − (S − NS)/

(MS − NS)], where S is the signal measured, NS is the non-specific binding signal and MS is the maximum binding signal observed with $btVEGF_{165}$ without compounds tested.

Acknowledgements

This work was supported by the Spanish Ministry of Science and Innovation (SAF 2006-01205, SAF 2009-09323, CTQ2008-0080/BQU and CTQ2011-22514), the CSIC (PIF 2005-80F0160 and PIE 2006-80I066) and the ANR (ANR-2012-BLAN-1533, project Salsa). M. I. G.-A. thanks the CSIC for a predoctoral fellowship (JAE-Predoc, from "Junta para la Ampliación de Estudios", co-financed by FSE), and the SEQT (Spanish Society of Therapeutic Chemistry) for the Ramón Madroñero award (XIV edition, 2009).

Notes and references

1 L. Coultas, K. Chawengsaksophak and J. Rossant, *Nature*, 2005, **438**, 937–945.
2 P. Carmeliet, *Nat. Med.*, 2003, **9**, 653–660.
3 N. Ferrara and R. S. Kerbel, *Nature*, 2005, **438**, 967–974.
4 R. Kerbel and J. Folkman, *Nat. Rev. Cancer*, 2002, **2**, 727–739.
5 N. Ferrara and T. Davis-Smyth, *Endocr. Rev.*, 1997, **18**, 4–25.
6 L. M. Ellis and D. J. Hicklin, *Nat. Rev. Cancer*, 2008, **8**, 579–591.
7 H. Gille, J. Kowalski, B. Li, J. LeCouter, B. Moffat, T. F. Zioncheck, N. Pelletier and N. Ferrara, *J. Biol. Chem.*, 2001, **276**, 3222–3230.
8 S. Kanno, N. Oda, M. Abe, Y. Terai, M. Ito, K. Shitara, K. Tabayashi, M. Shibuya and Y. Sato, *Oncogene*, 2000, **19**, 2138–2146.
9 B. Araújo Cautero Horta, A. C. Rennó Sodero and R. Bicca de Alencastro, *J. Mol. Graphics Modell.*, 2009, **28**, 287–296.
10 H. Takahashi and M. Shibuya, *Clin. Sci.*, 2005, **109**, 227–241.
11 C. Fischer, M. Mazzone, B. Jonckx and P. Carmeliet, *Nat. Rev. Cancer*, 2008, **8**, 942–956.
12 O. Feron, *Trends Pharmacol. Sci.*, 2004, **25**, 536–542.
13 J. Dancey and E. A. Sausville, *Nat. Rev. Drug Discovery*, 2003, **2**, 296–313.
14 N. Ferrara, K. J. Hillan, H.-P. Gerber and W. Novotny, *Nat. Rev. Drug Discovery*, 2004, **3**, 391–400.
15 G. Fuh, P. Wu, W.-C. Liang, M. Ultsch, C. V. Lee, B. Moffat and C. Wiesmann, *J. Biol. Chem.*, 2006, **281**, 6625–6631.
16 N. Ferrara, L. Damico, N. Shams, H. Lowman and R. Kim, *Retina*, 2006, **26**, 859–870.
17 K. H. Mayo, R. P. M. Dings, C. Flader, I. Nesmelova, B. Hargittai, D. W. J. van der Schaft, L. I. van Eijk, D. Walek, J. Haseman, T. R. Hoye and A. W. Griffioen, *J. Biol. Chem.*, 2003, **278**, 45746–45752.
18 D. Aviezer, S. Cotton, M. David, A. Segev, N. Khaselev, N. Galili, Z. Gross and A. Yayon, *Cancer Res.*, 2000, **60**, 2973–2980.
19 Y. Ueda, T. Yamagishi, K. Samata, H. Ikeya, N. Hirayama, H. Takashima, S. Nakaike, M. Tanaka and I. Saiki, *Mol. Cancer Ther.*, 2003, **2**, 1105–1111.
20 R. Binetruy-Tournaire, C. Demangel, B. Malavaud, R. Vassy, S. Rouyre, M. Kraemer, J. Plouet, C. Derbin, G. Perret and J. C. Mazie, *EMBO J.*, 2000, **19**, 1525–1533.
21 A. Starzec, R. Vassy, A. Martin, M. Lecouvey, M. Di Benedetto, M. Crépin and G. Y. Perret, *Life Sci.*, 2006, **79**, 2370–2381.
22 N. Ferrara, H. P. Gerber and J. LeCouter, *Nat. Med.*, 2003, **9**, 669–676.
23 L. Zilberberg, S. Shinkaruk, O. Lequin, B. Rousseau, M. Hagedorn, F. Costa, D. Caronzolo, M. Balke, X. Canron, O. Convert, G. Laïn, K. Gionnet, M. Gonçalves, M. Bayle, L. Bello, G. Chassaing, G. r. Deleris and A. Bikfalvi, *J. Biol. Chem.*, 2003, **278**, 35564–35573.
24 V. Goncalves, B. Gautier, P. Coric, S. Bouaziz, C. Lenoir, C. Garbay, M. Vidal and N. Inguimbert, *J. Med. Chem.*, 2007, **50**, 5135–5146.
25 H. Jia, S. Jezequel, M. Löhr, S. Shaikh, D. Davis, S. Soker, D. Selwood and I. Zachary, *Biochem. Biophys. Res. Commun.*, 2001, **283**, 164–173.
26 L. D. D'Andrea, G. Iaccarino, R. Fattorusso, D. Sorriento, C. Carannante, D. Capasso, B. Trimarco and C. Pedone, *Proc. Natl. Acad. Sci. U. S. A.*, 2005, **102**, 14215–14220.
27 J. W. B. Bainbridge, H. Jia, A. Bagherzadeh, D. Selwood, R. R. Ali and I. Zachary, *Biochem. Biophys. Res. Commun.*, 2003, **302**, 793–799.
28 B. Gautier, V. Goncalves, D. Diana, R. Di Stasi, F. Teillet, C. Lenoir, F. Huguenot, C. Garbay, R. Fattorusso, L. D. D'Andrea, M. Vidal and N. Inguimbert, *J. Med. Chem.*, 2010, **53**, 4428–4440.
29 B. Gautier, M. A. Miteva, V. Goncalves, F. Huguenot, P. Coric, S. Bouaziz, B. Seijo, J. F. Gaucher, I. Broutin, C. Garbay, A. Lesnard, S. Rault, N. Inguimbert, B. O. Villoutreix and M. Vidal, *Chem. Biol.*, 2011, **18**, 1631–1639.
30 C. Wiesmann, G. Fuh, H. W. Christinger, C. Eigenbrot, J. A. Wells and A. M. de Vos, *Cell*, 1997, **91**, 695–704.
31 V.-M. Leppänen, A. E. Prota, M. Jeltsch, A. Anisimov, N. Kalkkinen, T. Strandin, H. Lankinen, A. Goldman, K. Ballmer-Hofer and K. Alitalo, *Proc. Natl. Acad. Sci. U. S. A.*, 2010, **107**, 2425–2430.
32 B. A. Keyt, H. V. Nguyen, L. T. Berleau, C. M. Duarte, J. Park, H. Chen and N. Ferrara, *J. Biol. Chem.*, 1996, **271**, 5638–5646.
33 Y. A. Muller, B. Li, H. W. Christinger, J. A. Wells, B. C. Cunningham and A. M. de Vos, *Proc. Natl. Acad. Sci. U. S. A.*, 1997, **94**, 7192–7197.
34 Y. A. Muller, H. W. Christinger, B. A. Keyt and A. M. de Vos, *Structure*, 1997, **5**, 1325–1338.
35 B. Li, G. Fuh, G. Meng, X. Xin, M. E. Gerritsen, B. Cunningham and A. M. de Vos, *J.Biol. Chem.*, 2000, **275**, 29823–29828.

36 B. Pan, B. Li, S. J. Russell, J. Y. K. Tom, A. G. Cochran and W. J. Fairbrother, *J. Mol. Biol.*, 2002, **316**, 769–787.
37 M. I. García-Aranda, P. Marrero, B. Gautier, M. Martín-Martínez, N. Inguimbert, M. Vidal, M. T. García-López, M. A. Jiménez, R. González-Muñiz and M. J. Pérez de Vega, *Bioorg. Med. Chem.*, 2011, **19**, 1978–1986.
38 M. I. García-Aranda, Y. Mirassou, B. Gautier, M. Martín-Martínez, N. Inguimbert, M. Vidal, M. T. García-López, M. A. Jiménez, R. González-Muñiz and M. J. Pérez de Vega, *Bioorg. Med. Chem.*, 2011, **19**, 7526–7533.
39 L. D. D'Andrea, G. Iaccarino, R. Fattorusso, D. Sorriento, C. Carannante, D. Capasso, B. Trimarco and C. Pedone, *Proc. Natl. Acad. Sci. U. S. A.*, 2005, **102**, 14215–14220.
40 B. Ziaco, D. Diana, D. Capasso, R. Palumbo, V. Celentano, R. Di Stasi, R. Fattorusso and L. D. D'Andrea, *Biochem. Biophys. Res. Commun.*, 2012, **424**, 290–294.
41 A. Basile, A. Del Gatto, D. Diana, R. Di Stasi, A. Falco, M. Festa, A. Rosati, A. Barbieri, R. Franco, C. Arra, C. Pedone, R. Fattorusso, M. C. Turco and L. D. D'Andrea, *J. Med. Chem.*, 2011, **54**, 1391–1400.
42 Y. A. Muller, Y. Chen, H. W. Christinger, B. Li, B. C. Cunningham, H. B. Lowman and A. M. de Vos, *Structure*, 1998, **6**, 1153–1167.
43 Y. Yamazaki, K. Takani, H. Atoda and T. Morita, *J. Biol. Chem.*, 2003, **278**, 51985–51988.
44 K. Suto, Y. Yamazaki, T. Morita and H. Mizuno, *J. Biol. Chem.*, 2005, **280**, 2126–2131.
45 V. Muñoz and L. Serrano, *J. Mol. Biol.*, 1995, **245**, 275–296.
46 I. Tetko, J. Gasteiger, R. Todeschini, A. Mauri, D. Livingstone, P. Ertl, V. Palyulin, E. Radchenko, N. Zefirov, A. Makarenko, V. Tanchuk and V. Prokopenko, *J. Comput. Aided Mol. Des.*, 2005, **19**, 453–463.
47 VCCLAB (Virtual Computational Chemistry Laboratory), 2005.
48 N. E. Shepherd, H. N. Hoang, V. S. Desai, E. Letouze, P. R. Young and D. P. Fairlie, *J. Am. Chem. Soc.*, 2006, **128**, 13284–13289.
49 N. L. Mills, M. D. Daugherty, A. D. Frankel and R. K. Guy, *J. Am. Chem. Soc.*, 2006, **128**, 3496–3497.
50 K. K. Khoo, M. J. Wilson, B. J. Smith, M.-M. Zhang, J. Gulyas, D. Yoshikami, J. E. Rivier, G. Bulaj and R. S. Norton, *J. Med. Chem.*, 2011, **45**, 7558–7566.
51 *Solid-Phase Synthesis. A practical guide.*, ed. S. A. Kates and F. Albericio, Marcel Dekker INC., New York. Basel, 2000.
52 E. Valeur and M. Bradley, *Chem. Soc. Rev.*, 2009, **38**, 606–631.
53 D. Andreu, S. Ruiz, C. Carreño, J. Alsina, F. Albericio, M. A. Jimenez, N. de la Figuera, R. Herranz, M. T. Garcia-López and R. González-Muñiz, *J. Am. Chem. Soc.*, 1997, **119**, 10579–10586.
54 N. Vale, J. Matos, R. Moreira and P. Gomes, *J. Am. Soc. Mass Spectrom.*, 2008, **19**, 1476–1490.
55 P. Barral, M. L. Tejera, M. Á. Treviño, E. Batanero, M. Villalba, M. Bruix and R. Rodríguez, *Protein Expression Purif.*, 2004, **37**, 336–343.
56 D. S. Wishart, B. D. Sykes and F. M. Richards, *J. Mol. Biol.*, 1991, **222**, 311–333.
57 D. S. Wishart, C. G. Bigam, A. Holm, R. S. Hodges and B. D. Sykes, *J. Biomol. NMR*, 1995, **5**, 67–81.
58 R. Vila, I. Ponte, P. Suau, M. A. Jiménez and M. Rico, *Protein Sci.*, 2000, **9**, 627–636.
59 M. A. Jiménez, A. C. Barrachi-Saccilotto, E. Valdivia, M. Maqueda and M. Rico, *J. Pept. Sci.*, 2005, **11**, 29–36.
60 V. Goncalves, B. Gautier, C. Garbay, M. Vidal and N. Inguimbert, *Anal. Biochem.*, 2007, **366**, 108–110.
61 A. Chakrabartty, A. J. Doig and R. L. Baldwin, *Proc. Natl. Acad. Sci. U. S. A.*, 1993, **90**, 11332–11336.
62 R. P. Cheng, P. Girinath and R. Ahmad, *Biochemistry*, 2007, **46**, 10528–10537.
63 C. M. Santiveri, D. Pantoja-Uceda, M. Rico and M. A. Jimenez, *Biopolymers*, 2005, **79**, 150–162.
64 *Program TOPSPIN. NMR Data Acquisition and Processing Software*, Bruker Biospin, Karlsruhe, Germany.
65 D. S. Wishart, C. G. Bigam, J. Yao, F. Abildgaard, H. J. Dyson, E. Oldfield, J. L. Markley and B. D. Sykes, *J. Biomol. NMR*, 1995, **6**, 135–140.
66 K. Wuthrich, *NMR of Proteins and Nucleic Acids*, John Wiley & Sons, New York, 1986.
67 K. Wuthrich, M. Billeter and W. Braun, *J. Mol. Biol.*, 1984, **180**, 715–740.
68 T. D. Goddard and D. G. Kneller, *Sparky 3 NMR Assignment Program*, San Francisco, USA.
69 G. Cornilescu, F. Delaglio and A. Bax, *J. Biomol. NMR*, 1999, **13**, 289–302.
70 P. Güntert, C. Mumenthaler and K. Wüthrich, *J. Mol. Biol.*, 1997, **273**, 283–298.
71 R. Koradi, M. Billeter and K. Wuthrich, MOLMOL program, *J. Mol. Graph.*, 1996, **14**, 29–32.